

# KernelNet: A Data-Dependent Kernel Parameterization for Deep Generative Modeling

**Yufan Zhou,**  
yufanzho@buffalo.edu  
Department of CSE  
University at Buffalo, SUNY

**Changyou Chen**  
changyou@buffalo.edu  
Department of CSE  
University at Buffalo, SUNY

**Jinhui Xu**  
jinhui@buffalo.edu  
Department of CSE  
University at Buffalo, SUNY

February 23, 2021

## Abstract

Learning with kernels is an often resorted tool in modern machine learning. Standard approaches for this type of learning use a predefined kernel that requires careful selection of hyperparameters. To mitigate this burden, we propose in this paper a framework to construct and learn a data-dependent kernel based on random features and implicit spectral distributions (Fourier transform of the kernel) parameterized by deep neural networks. We call the constructed network *KernelNet*, and apply it for deep generative modeling in various scenarios, including variants of the MMD-GAN and an implicit Variational Autoencoder (VAE), the two popular learning paradigms in deep generative models. Extensive experiments show the advantages of the proposed KernelNet, consistently achieving better performance compared to related methods.

## 1 Introduction

Kernels are important tools in machine learning, and find applications in a wide range of models, from one of the earliest models, support vector machine (SVM), to the latest work on statistical testing with Maximum Mean Discrepancy (MMD) and various applications in deep generative models including generative adversarial networks (GAN) and variational autoencoders (VAE) [13, 29]. These models are built by either restricting the solution space to a Reproducing Kernel Hilbert Space (RKHS) induced by a kernel, or adopting the MMD metric as the objective functions that require specified kernels in their MMDs. Other kernel-based methods such as those proposed by Feng et al. [5], Yin and Zhou [28] rely on special kernels for computing estimations of some quantities such as gradients.

A not-so-desirable issue of the aforementioned kernel-based methods, however, is the need of selecting appropriate hyperparameters, *e.g.*, the bandwidth of an RBF kernel. These hyperparameters are critical for obtaining good performance, and manual selection often leads to sub-optimal solutions. Preliminary works have been proposed to mitigate

this problem. For example, Gönen and Alpaydin [6] proposed to learn a combination of some predefined kernels. Alternatively, some other recent works focus on learning kernels based on random features or the corresponding spectral distributions when taking Fourier transform for the kernel [2, 18, 26] (see Section 3.1 for a more detailed description).

As a principled approach, in this paper, we propose a new kernel-learning paradigm by defining a more expressive yet easy-to-be-handled distribution of the corresponding kernel in the spectral domain, and by parameterizing it as a data-dependent implicit distribution with deep neural networks (DNNs). We call the resulting network *KernelNet*, call the kernel corresponds to the data-dependent distribution *data-dependent kernel*. Specifically, based on related kernel theory, we formulate a kernel in the spectral domain as an expectation of a function w.r.t. some random features, whose distribution is called the spectral distribution. The particular function and the spectral distribution then allow us to impose expressive DNN structures to parameterize the kernel. We propose a novel and expressive way of parameterizing the spectral distribution as a data-dependent implicit distribution. This is distinct from a recent work [14] which modeled the spectral distribution as a data-independent distribution, and thus is less expressive. Our method is more general than Li et al. [14], a special case of ours. Moreover, the data-dependent kernel component in KernelNet could lead to performance improvement over data-independent parameterization, as evidenced by our experiments.

The proposed KernelNet is quite flexible to be applied to existing models. We apply it to Deep Generative Models (DGMs) based on two representative DGM frameworks, the Maximum Mean Discrepancy GAN (MMD-GAN) [13] and the Info-VAE [29]. Specifically, *i)* we apply our kernel parameterization to several state-of-the-art MMD-GAN variants, including the spectral normalized MMD-GAN (SN-MMD-GAN) [1, 17] and the scale MMD-GAN (SMMD-GAN) [1], which allows us to learn the models and the KernelNet simultaneously. We show theoretically that our proposed models satisfy weak topology, an important property to ensure the robustness of optimization procedures. *ii)* We propose an implicit VAE model, where an MMD-regularizer is incorporated into the objective of VAE, following the Info-VAE framework. Our model is implicit in the sense that the variational distribution is parameterized as an implicit distribution implemented by a conditional generator, compared to the typical Gaussian assumption in standard VAE. This enables us to model a much more flexible latent space. The learning is done by adopting the Stein gradient estimator to optimize the implicit distribution [15]. Extensive experiments are performed to evaluate our proposed framework. The results suggest that our framework achieves significant improvement over existing ones.

## 2 Preliminaries

We review MMD-GAN and Info-VAE, two DGMs where our proposed data-dependent kernels apply.

### 2.1 MMD-GAN

Generative Adversarial Network (GAN) is one of the most popular and powerful generative models in deep learning. It consists of a generator and a discriminator. The generator generate samples by transforming a simple noise distribution to an implicit data distribution

$\mathbb{Q}_\theta$ , *i.e.*, one can easily generate samples from the distribution, but without the knowledge of the density function. The discriminator is trained to distinguish the true training data distribution  $\mathbb{P}$  and the implicit distribution  $\mathbb{Q}_\theta$  induced by the generator. The generator, on the other hand, is trained to fool the discriminator. At equilibrium, the generator is able to generate samples that are distributed as the true data distribution  $\mathbb{P}$ .

MMD-GAN achieves this by minimizing the maximum mean discrepancy (MMD) between two probability measures, the data and model distributions.

**Maximum Mean Discrepancy [1]** The Maximum Mean Discrepancy (MMD) between two probability measures  $\mathbb{P}$  and  $\mathbb{Q}$  is defined as:

$$\text{MMD}_k(\mathbb{P}, \mathbb{Q}) = \sup_{f: \|f\|_{\mathcal{H}} \leq 1} \mathbb{E}_{\mathbf{x} \sim \mathbb{P}}[f(\mathbf{x})] - \mathbb{E}_{\mathbf{y} \sim \mathbb{Q}}[f(\mathbf{y})]$$

where  $\mathcal{H}$  is a Reproducing Kernel Hilbert Space (RKHS) and  $f$  is a function in this RKHS.

For an RKHS induced by kernel  $k$ , MMD can be computed using the following equation:

$$\text{MMD}_k^2(\mathbb{P}, \mathbb{Q}) = \mathbb{E}_{\mathbf{x}, \mathbf{x}' \sim \mathbb{P}}[k(\mathbf{x}, \mathbf{x}')] - 2\mathbb{E}_{\mathbf{x} \sim \mathbb{P}, \mathbf{y} \sim \mathbb{Q}}[k(\mathbf{x}, \mathbf{y})] + \mathbb{E}_{\mathbf{y}, \mathbf{y}' \sim \mathbb{Q}}[k(\mathbf{y}, \mathbf{y}')].$$

For a characteristic kernel,  $\text{MMD}_k(\mathbb{P}, \mathbb{Q}) = 0$  if and only if  $\mathbb{P} = \mathbb{Q}$ . Thus, MMD can be used as a way of measuring the similarity of distributions or as a training objective. Li et al. [13] proposes MMD-GAN, where the kernel is defined as a composition of an injective function  $h_\phi$  for feature extraction and a kernel function  $k$  for kernel evaluation, *e.g.*,  $\tilde{k} = k \circ h_\phi$ . Note that  $\tilde{k}$  is also a valid kernel function. For example, if  $k$  is the Gaussian kernel,  $\tilde{k}(\mathbf{x}, \mathbf{y}) = \exp(-\|h_\phi(\mathbf{x}) - h_\phi(\mathbf{y})\|^2)$  is also a kernel.

In addition, a generator  $f_\theta$  parameterized by  $\theta$  is introduced for data generation, whose generated data are expected to match the training data in distribution by minimizing the corresponding MMD. Specifically, let  $\mathbb{P}$  represent the training data distribution and  $\mathbb{Q}_\theta$  the implicit output distribution induced by the generator. The objective of MMD-GAN is formulated as:

$$\min_{\theta} \max_{\phi} \text{MMD}_{k \circ h_\phi}^2(\mathbb{P}, \mathbb{Q}).$$

In MMD-GAN, both  $h_\phi$  and  $f_\theta$  are parameterized by neural networks. Because of the min-max adversarial training,  $\mathbb{Q}_\theta$  will eventually match  $\mathbb{P}$  in theory. Some improvements have also been proposed. One particular variant we are focusing on is called Scaled Maximum Mean Discrepancy.

**Scaled Maximum Mean Discrepancy [1]** The Scaled Maximum Mean Discrepancy is defined as:

$$\text{SMMD}_{\mu, k, \lambda}(\mathbb{P}, \mathbb{Q}) := \sup_{f: \|f\|_{\mathcal{H}} / \sigma_{\mu, k, \lambda} \leq 1} \mathbb{E}_{\mathbf{x} \sim \mathbb{P}}[f(\mathbf{x})] - \mathbb{E}_{\mathbf{x} \sim \mathbb{Q}}[f(\mathbf{x})] = \sigma_{\mu, k, \lambda} \text{MMD}_k(\mathbb{P}, \mathbb{Q}),$$

$$\text{where } \sigma_{\mu, k, \lambda} := \left( \lambda + \int k(\mathbf{x}, \mathbf{x}) d\mathbb{P}(\mathbf{x}) + \sum_{i=1}^d \int \frac{\partial^2 k(\mathbf{y}_1, \mathbf{y}_2)}{\partial \mathbf{y}_{1i} \partial \mathbf{y}_{2i}} \Big|_{(\mathbf{y}_1, \mathbf{y}_2) = (\mathbf{x}, \mathbf{x})} d\mathbb{P}(\mathbf{x}) \right)^{-1/2}.$$

Replacing the objective function of MMD-GAN by SMMD leads to the SMMD-GAN [1]. One useful and important method in training MMD-GAN is spectral normalization [17], which can control the Lipschitz constant of the injective function  $h_\phi$  and lead to stable

training and better performance. Spectral normalization normalizes the weight matrix  $\mathbf{W}$  by its spectral norm  $\sigma(\mathbf{W})$ , *i.e.*,  $\bar{\mathbf{W}} = \mathbf{W} / \sigma(\mathbf{W})$  with  $\sigma(\mathbf{W}) := \max_{\mathbf{h}: \|\mathbf{h}\|_2=1} \|\mathbf{W} \mathbf{h}\|_2 = \max_{\|\mathbf{h}\|_2 \leq 1} \|\mathbf{W} \mathbf{h}\|_2$ . The Lipschitz constant of  $h_\phi$  is thus bounded from above by 1. MMD-GAN with spectral normalization is called SN-MMD-GAN, whereas SMMD-GAN with spectral parameterization [1, 17], defined as  $\bar{\mathbf{W}} = \gamma \mathbf{W} / \sigma(\mathbf{W})$  with  $\gamma$  being a learnable parameter, is called SN-SMMD-GAN.

## 2.2 Info-VAE

VAE and its variants are another family of DGMs where latent spaces are defined with posterior distributions. Specifically, define a generative process for an observation  $\mathbf{x} \in \mathbb{R}^D$ , starting from the corresponding latent variable  $\mathbf{z} \in \mathbb{R}^d$ , as:  $\mathbf{x} | \mathbf{z} \sim p_\theta(\mathbf{x} | \mathbf{z})$  with  $\mathbf{z} \sim p(\mathbf{z})$  and  $\theta$  the parameter of the generative model. For efficient inference of  $\mathbf{z}$ , VAE [11, 19] defines an inference network (or encoder) to generate  $\mathbf{z}$  from  $\mathbf{x}$ , with the corresponding generation distribution being  $q_\phi(\mathbf{z} | \mathbf{x})$  parameterized by  $\phi$  (also called variational distribution).

Info-VAE [29] is a generalization of VAE by introducing an information-theoretic regularizer into the VAE framework. The objective is:

$$\max_{\phi, \theta} - \mathbb{E}_{q_\phi(\mathbf{z})} \{ \text{KL}[q_\phi(\mathbf{x} | \mathbf{z}) \| p_\theta(\mathbf{x} | \mathbf{z})] \} + \alpha \mathbf{I}_{q_\phi}(\mathbf{x}, \mathbf{z}) - \lambda \text{KL}[q_\phi(\mathbf{z}) \| p(\mathbf{z})], \quad (1)$$

where  $\mathbf{I}_{q_\phi}(\mathbf{x}, \mathbf{z})$  is the mutual information between  $\mathbf{x}$  and  $\mathbf{z}$  that is defined as:

$$\mathbf{I}_{q_\phi}(\mathbf{x}, \mathbf{z}) = \mathbb{E}_{q(\mathbf{x})} \{ \text{KL}[q_\phi(\mathbf{z} | \mathbf{x}) \| q_\phi(\mathbf{z})] \}.$$

Note that both KL and MMD describe difference between distributions. Thus in our approach, we propose to use an MMD regularizer instead of mutual information, some discussions can be found in Appendix E. Furthermore, our model considers an implicit setting where  $q_\phi$  is defined as an implicit distribution, making our model more expressive.

## 3 KernelNet for Learning Deep Generative Models

### 3.1 The Proposed KernelNet

To alleviate the difficulties with pre-defined kernels such as hyperparameter selection, we propose KernelNet, a principled way to parameterize a kernel with a deep neural network (DNN). Our method improves the recent work Li et al. [14] by making the kernel data-dependent and applying it to different DGMs, which has shown to be able to boost model performance.

We start with a classic result on positive definite functions [20], stated in Lemma 1.

**Lemma 1 (Rudin [20])** *A continuous function  $\kappa(\mathbf{z})$  in  $\mathbb{R}^d$  is positive definite if and only if it is the Fourier transform of a non-negative measure.*

Let  $\zeta_\omega(\mathbf{z}) = e^{j\omega^\top \mathbf{z}}$ . By Lemma 1 and [18], a kernel such that  $\kappa(\mathbf{z}_1, \mathbf{z}_2) = \tilde{\kappa}(\mathbf{z}_1 - \mathbf{z}_2)$  can be represented as:

$$\kappa(\mathbf{z}_1, \mathbf{z}_2) = \int_{\mathbb{R}^d} p(\omega) e^{j\omega^\top (\mathbf{z}_1 - \mathbf{z}_2)} d\omega = \mathbb{E}_\omega [\zeta_\omega(\mathbf{z}_1) \zeta_\omega(\mathbf{z}_2)^*], \quad (2)$$

where  $j$  is an indeterminate satisfying  $j^2 = -1$ , and “ $*$ ” denotes the conjugate transpose. The kernel representation (2) directly allows us to construct an unbiased estimator for  $\kappa(\cdot, \cdot)$  by introducing any valid distribution  $p(\boldsymbol{\omega})$  for the augmented variable  $\boldsymbol{\omega}$ , called the *spectral distribution*. This distribution will be parameterized by an implicit distribution with a DNN, described later. In the following, we first reformulate (2) into two equivalent forms for the purposes of analysis and algorithm design, respectively. Because the probability density function and kernel function are real-valued, by Euler’s formula, we have

**Proposition 2** *Let  $\boldsymbol{\omega}$  be drawn from some spectral distribution  $p(\boldsymbol{\omega})$ , and  $b$  be drawn uniformly from  $[0, 2\pi]$ . The real-valued kernel in (2) can be reformulated into the following two forms:*

$$\kappa(\mathbf{z}_1, \mathbf{z}_2) = \mathbb{E}_{\boldsymbol{\omega} \sim p(\boldsymbol{\omega})} \{ \cos[\boldsymbol{\omega}^\top (\mathbf{z}_1 - \mathbf{z}_2)] \} \quad (3)$$

$$= \mathbb{E}_{\boldsymbol{\omega} \sim p(\boldsymbol{\omega}), b \sim \mathcal{U}[0, 2\pi]} [2 \cos(\boldsymbol{\omega}^\top \mathbf{z}_1 + b) \cos(\boldsymbol{\omega}^\top \mathbf{z}_2 + b)] . \quad (4)$$

Detailed derivations can be found in Appendix A. In the above two representation, (3) is more convenient for analysis, and (4) is found more stable in implementation (algorithm).

To enhance the expression power, we can make the distribution  $p(\boldsymbol{\omega})$  complex enough and learnable by parameterizing it with a DNN that induces an implicit distribution, as in generative adversarial networks (GAN) [7]. Specifically, we rewrite  $p(\boldsymbol{\omega})$  as  $p_{\psi_1}(\boldsymbol{\omega})$  with parameter  $\psi_1$ . A sample  $\boldsymbol{\omega}$  from  $p_{\psi_1}(\cdot)$  is modeled as the following generating process:

$$\boldsymbol{\omega}_{\psi_1} = g_{\psi_1}(\boldsymbol{\epsilon}), \quad \boldsymbol{\epsilon} \sim \mathcal{N}(\mathbf{0}, \mathbf{I}) , \quad (5)$$

where  $g_{\psi_1}(\boldsymbol{\epsilon})$  denotes the output of a DNN parameterized by  $\psi_1$  with the input  $\boldsymbol{\epsilon}$  drawn from some simple distributions like standard Gaussian or uniform distributions.

**Extension to data-dependent kernels** Although the above kernel parameterization is flexible enough to represent a rich family of implicit spectral distributions, it can be further extended by introducing a data-dependent spectral distribution. By data-dependent spectral distribution, we mean that there are some kernels satisfying (2), whose spectral distributions  $p(\boldsymbol{\omega})$  depend on the data pair  $(\mathbf{z}_1, \mathbf{z}_2)$ , *i.e.*, there exists a  $p(\boldsymbol{\omega} | \mathbf{z}_1, \mathbf{z}_2)$  for each pair  $(\mathbf{z}_1, \mathbf{z}_2)$  and a marginal distribution  $p(\boldsymbol{\omega})$  across the whole dataset.

We use the term data-dependent because of two reasons: 1) The marginal distribution  $p(\boldsymbol{\omega})$  depends on specific datasets, which could induce different formulas on different datasets; 2) For a given input pair  $(\mathbf{z}_1, \mathbf{z}_2)$ , the conditional distributions and the kernel values  $\kappa(\mathbf{z}_1, \mathbf{z}_2)$  depend the input pair  $(\mathbf{z}_1, \mathbf{z}_2)$ . Thus  $\mathbf{z}_1 - \mathbf{z}_2 = \mathbf{z}_3 - \mathbf{z}_4$  does not necessarily imply  $\kappa(\mathbf{z}_1, \mathbf{z}_2) = \kappa(\mathbf{z}_3, \mathbf{z}_4)$ . Proposition 3 shown this setting is possible.

**Proposition 3** *There exist some positive definite kernels, which can be expressed as:*

$$\kappa(\mathbf{z}_1, \mathbf{z}_2) = \int_{R^d} p(\boldsymbol{\omega} | \mathbf{z}_1, \mathbf{z}_2) e^{j \boldsymbol{\omega}^\top (\mathbf{z}_1 - \mathbf{z}_2)} d\boldsymbol{\omega}$$

The proof is provided in Appendix B. One example of such a kernel is a symmetric positive definite kernel defined on manifold  $M \subset R^d$ , whose value depends on the geodesic distance between two points rather than the Euclidean distance.

Some practical tricks can also be understood in the sense of data-dependent kernels. For example, using median heuristic bandwidth can be seen as dividing  $\mathbf{z}_1$  and  $\mathbf{z}_2$  by some

data dependent quantity, denoted as  $\delta_{\mathbf{z}_1, \mathbf{z}_2}$ . That is, if one defines  $\tilde{\mathbf{z}}_1 = \mathbf{z}_1 / \delta_{\mathbf{z}_1, \mathbf{z}_2}$  and  $\tilde{\mathbf{z}}_2 = \mathbf{z}_2 / \delta_{\mathbf{z}_1, \mathbf{z}_2}$ , and substitutes them into (2), one ends up:

$$\tilde{\kappa}(\mathbf{z}_1, \mathbf{z}_2) \triangleq \int_{R^d} p(\boldsymbol{\omega}) e^{j\boldsymbol{\omega}^\top (\tilde{\mathbf{z}}_1 - \tilde{\mathbf{z}}_2)} d\boldsymbol{\omega} = \int_{R^d} \tilde{p}(\tilde{\boldsymbol{\omega}}) e^{j\tilde{\boldsymbol{\omega}}^\top (\mathbf{z}_1 - \mathbf{z}_2)} d\tilde{\boldsymbol{\omega}}, \quad (6)$$

where  $\tilde{\boldsymbol{\omega}} = \boldsymbol{\omega} / \delta_{x,y}$ , and  $\tilde{p}(\tilde{\boldsymbol{\omega}}) = \delta_{x,y} p(\boldsymbol{\omega})$ . The kernel definition in (6) is similar to a kernel with a data-dependent spectral distribution  $\tilde{p}(\tilde{\boldsymbol{\omega}})$ .

**Constructing a data-dependent kernel network** To construct a data-dependent kernel network, we extend (5) to the following generative process:  $\boldsymbol{\omega}_{\psi_2, \mathbf{z}_1, \mathbf{z}_2} = g_{\psi_2}(\boldsymbol{\epsilon}, \mathbf{z}_1, \mathbf{z}_2)$  with  $\boldsymbol{\epsilon} \sim \mathcal{N}(\mathbf{0}, \mathbf{I})$ . Note that such an implicit construction requires multiple noise samples to approximate the distribution of  $\boldsymbol{\omega}_{\psi_2, \mathbf{z}_1, \mathbf{z}_2}$  for each  $(\mathbf{z}_1, \mathbf{z}_2)$  pair, which could be time consuming when minibatch sizes are large. To tackle this issue, we propose to decompose a kernel into an explicit data-independent component and an implicit data-dependent component. Note that such a decomposition still guarantees the implicitity of the overall kernel, and thus will not lose generalization. Specifically, we use the reparameterization trick to define a data-dependent sampling process, *i.e.*, a sample from the data-dependent spectral distribution, denoted by  $\boldsymbol{\omega}'_{\psi_2, \mathbf{z}_1, \mathbf{z}_2}$  as it depends on  $(\psi_2, \mathbf{z}_1, \mathbf{z}_2)$ :

$$\boldsymbol{\omega}'_{\psi_2, \mathbf{z}_1, \mathbf{z}_2} = \boldsymbol{\mu}_{\psi_2, \mathbf{z}_1, \mathbf{z}_2} + \boldsymbol{\epsilon} \odot \boldsymbol{\sigma}_{\psi_2, \mathbf{z}_1, \mathbf{z}_2}, \quad \boldsymbol{\epsilon} \sim \mathcal{N}(\mathbf{0}, \mathbf{I}), \quad (7)$$

where  $\boldsymbol{\mu}_{\psi_2, \mathbf{z}_1, \mathbf{z}_2}$  and  $\boldsymbol{\sigma}_{\psi_2, \mathbf{z}_1, \mathbf{z}_2}$  are outputs from a DNN parameterized by  $\psi_2$ ;  $\odot$  denotes the element-wise multiplication. Because this may lead to an asymmetric kernel, we can further construct a symmetric kernel by simply setting  $\boldsymbol{\omega}_{\psi_2, \mathbf{z}_1, \mathbf{z}_2} = (\boldsymbol{\omega}'_{\psi_2, \mathbf{z}_1, \mathbf{z}_2} + \boldsymbol{\omega}'_{\psi_2, \mathbf{z}_2, \mathbf{z}_1})/2$ . For the data-independent component, we adopt the implicit representation defined in (5). Consequently, the overall KernelNet is constructed as:

$$\kappa_{\psi}(\mathbf{z}_1, \mathbf{z}_2) \triangleq \kappa_{\psi_1}(\mathbf{z}_1, \mathbf{z}_2) + \kappa_{\psi_2}(\mathbf{z}_1, \mathbf{z}_2), \quad \text{where} \quad (8)$$

$$\begin{aligned} \kappa_{\psi_1}(\mathbf{z}_1, \mathbf{z}_2) &= \mathbb{E}_{\boldsymbol{\omega}_{\psi_1}, b} \left[ 2 \cos(\boldsymbol{\omega}_{\psi_1}^\top \mathbf{z}_1 + b) \cos(\boldsymbol{\omega}_{\psi_1}^\top \mathbf{z}_2 + b) \right], \\ \kappa_{\psi_2}(\mathbf{z}_1, \mathbf{z}_2) &= \mathbb{E}_{\boldsymbol{\omega}_{\psi_2}, b} \left[ 2 \cos(\boldsymbol{\omega}_{\psi_2, \mathbf{z}_1, \mathbf{z}_2}^\top \mathbf{z}_1 + b) \cos(\boldsymbol{\omega}_{\psi_2, \mathbf{z}_1, \mathbf{z}_2}^\top \mathbf{z}_2 + b) \right]. \end{aligned} \quad (9)$$

The network structure is illustrated in Figure 1. In implementation, the expectations are approximated by samples, *e.g.*:

$$\mathbb{E}_{\boldsymbol{\omega}_{\psi_1}, b} \left[ 2 \cos(\boldsymbol{\omega}_{\psi_1}^\top \mathbf{z}_1 + b) \cos(\boldsymbol{\omega}_{\psi_1}^\top \mathbf{z}_2 + b) \right] \approx \frac{2}{N} \sum_{i=1}^N \cos(\boldsymbol{\omega}_{\psi_1 i}^\top \mathbf{z}_1 + b_i) \cos(\boldsymbol{\omega}_{\psi_1 i}^\top \mathbf{z}_2 + b_i),$$

where all  $\boldsymbol{\omega}_{\psi_1 i}$ 's are samples from the spectral distributions  $p(\boldsymbol{\omega}_{\psi_1})$  through (5). In addition,  $b_i$ 's are drawn from  $p_b = \mathcal{U}[0, 2\pi]$ . Since the construction is implicit with no stochastic intermediate nodes, standard back-propagation can be applied for efficient end-to-end training. Lemma 4 below guarantees that the output of the KernelNet (8) is still a legitimate kernel.

**Lemma 4 (Shawe-Taylor and Cristianini [24])** *Let  $\kappa_1(\mathbf{z}_1, \mathbf{z}_2)$  and  $\kappa_2(\mathbf{z}_1, \mathbf{z}_2)$  be two kernels over  $R^d \times R^d$ , then  $\kappa'(\mathbf{z}_1, \mathbf{z}_2) \triangleq \kappa_1(\mathbf{z}_1, \mathbf{z}_2) + \kappa_2(\mathbf{z}_1, \mathbf{z}_2)$  is also a kernel.*

It is worth noting that if we remove the data-dependent component, the kernel reduces to the one in Li et al. [14]. We will show in the experiments that the data-dependent component actually plays an important role, and can lead to performance improvement.

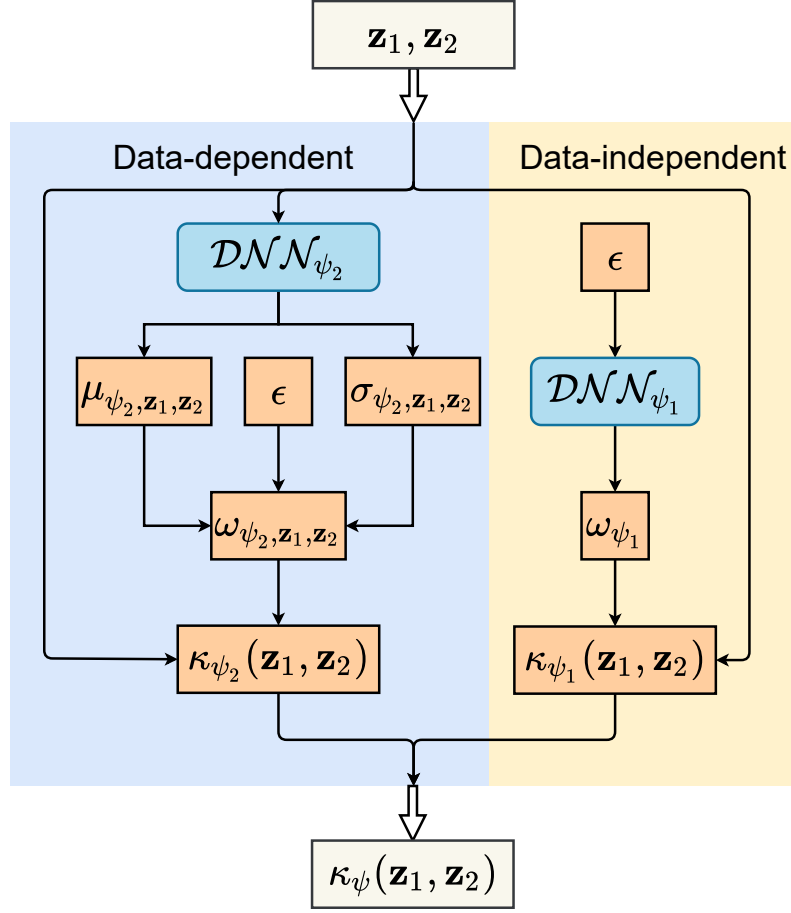


Figure 1: Structure of the proposed KernelNet, where  $\epsilon \sim \mathcal{N}(\mathbf{0}, \mathbf{I})$ .

### 3.2 KernelNet for MMD-GAN

In this section, we incorporate the proposed KernelNet into learning the MMD-GAN model. We seek to develop an algorithm to jointly optimize both the KernelNet and the MMD-GAN model. A straightforward way is to replace the standard kernel in MMD-GAN with the proposed data-dependent kernel (8). However, as the standard MMD-GAN fails to satisfy *continuity in weak topology*, a property that ensures metric discontinuity in a topological space, it is unclear whether the variant with our KernelNet would satisfy the property. To this end, we first define *continuity in weak topology*.

**Continuity in weak topology [1]**  $\text{MMD}_k(\mathbb{Q}, \mathbb{P})$  is said to endow continuity in weak topology if  $\mathbb{Q} \xrightarrow{D} \mathbb{P}$  implies  $\text{MMD}_{k_\nu}(\mathbb{Q}_n, \mathbb{P}) \rightarrow 0$ , where  $\xrightarrow{D}$  means convergence in distribution.

Continuity in weak topology in MMD-GAN is important because it was discovered by Arbel et al. [1] that continuity in the weak topology makes the loss provide better signal to the generator as  $\mathbb{Q}$  approaches  $\mathbb{P}$ . Arbel et al. [1] also finds that the optimized MMD distance in MMD-GAN is not continuous in the weak topology, leading to training

instability and poor performance. To alleviate this problem, a number of methods have been introduced, *e.g.*, through weight-clipping [13], spectral normalization [17], gradient penalty [8], and adopting a scaled objective (SMMD-GAN) [1]. Fortunately, we can prove that adopting our KernelNet in MMD-GAN leads to continuity in weak topology, based on the recent work Arbel et al. [1].

**Proposition 5** *By parameterizing the kernel with our KernelNet  $\kappa_{\psi}(\mathbf{z}_1, \mathbf{z}_2) = \kappa_{\psi_1}(\mathbf{z}_1, \mathbf{z}_2) + \kappa_{\psi_2}(\mathbf{z}_1, \mathbf{z}_2)$ ,  $\text{MMD}_{k_{\psi}}(\mathbb{P}, \mathbb{Q})$  is continuous in the weak topology if the following are satisfied:*

$$\begin{aligned} \mathbb{E}_{\omega_{\psi_1}} [\|\omega_{\psi_1}\|^2] &< \infty, \quad \mathbb{E}_{\omega_{\psi_2, \mathbf{z}_1, \mathbf{z}_2}} [\|\omega_{\psi_2, \mathbf{z}_1, \mathbf{z}_2}\|^2] < \infty, \\ \mathbb{E}_{\omega_{\psi_2, \mathbf{z}_1, \mathbf{z}_2}} \left[ \left\| \frac{\partial \omega_{\psi_2, \mathbf{z}_1, \mathbf{z}_2}}{\partial \mathbf{z}_1} - \frac{\partial \omega_{\psi_2, \mathbf{z}_1, \mathbf{z}_2}}{\partial \mathbf{z}_2} \right\|_{\mathcal{F}} \right] &< \infty, \quad \sup_{\phi \in \Phi} \|h_{\phi}\|_{\text{Lip}} < \infty \end{aligned} \quad (10)$$

where  $\|\cdot\|_{\mathcal{F}}$  denotes the Frobenius norm of a matrix,  $h_{\phi}$  is the injective function in MMD-GAN, *i.e.*,  $\mathbf{z} = h_{\phi}(\mathbf{x})$ , and  $\|h_{\phi}\|_{\text{Lip}}$  denotes its Lipschitz constant.

The proof can be found in Appendix C. Based on Proposition 5, we propose two variants of the MMD-GAN model, respectively corresponding to the SN-MMD-GAN [1, 17] and the SMMD-GAN [1], by incorporating the conditions in Proposition 5 into the objective functions.

**MMD-GAN with the KernelNet** By adopting spectral normalization and the method of Lagrange multipliers to regularize the conditions in Proposition 5, we propose SN-MMD-GAN-DK. Note that  $\sup_{\phi \in \Phi} \|h_{\phi}\|_{\text{Lip}} < \infty$  is satisfied because of the spectral normalization operation, which normalizes the weight matrix during the training process. The objective is defined as:

$$\min_{\theta} \max_{\phi, \psi} \text{MMD}_{k_{\phi, \psi}}^2(\mathbb{P}, \mathbb{Q}_{\theta}) \pm \Omega(\theta, \phi, \psi), \quad (11)$$

where

$$\Omega(\theta, \phi, \psi) \triangleq \alpha_1 \mathbb{E}_{\omega_{\psi_1}} [\|\omega_{\psi_1}\|^2] + \mathbb{E}_{\omega_{\psi_2, \mathbf{z}_1, \mathbf{z}_2}} [\alpha_2 \|\omega_{\psi_2, \mathbf{z}_1, \mathbf{z}_2}\|^2 + \alpha_3 \left\| \frac{\partial \omega_{\psi_2, \mathbf{z}_1, \mathbf{z}_2}}{\partial \mathbf{z}_1} - \frac{\partial \omega_{\psi_2, \mathbf{z}_1, \mathbf{z}_2}}{\partial \mathbf{z}_2} \right\|_{\mathcal{F}}]$$

$\pm$  in (11) means we use “+” when minimizing w.r.t.  $\theta$  and use “-” when maximizing w.r.t.  $(\phi, \psi)$ , according to Proposition 5.

**Scaled MMD-GAN with the KernelNet** Similarly, based on the SMMD-GAN model by Arbel et al. [1], we propose our variant by incorporating the conditions in Proposition 5 into the SMMD framework in Definition 2.1. First, we have:

**Proposition 6** *With the proposed data-dependent KernelNet (8), the SMMD-DK framework in Definition 2.1 can be formulated and simplified as:*

$$\text{SMMD-DK}_{k_{\psi, \phi}, \lambda}(\mathbb{P}, \mathbb{Q}) := \sigma_{k_{\psi, \phi}, \lambda} \text{MMD}_{k_{\psi}}(\mathbb{P}, \mathbb{Q}), \quad \text{where}$$

$$\sigma_{k_{\psi, \phi}, \lambda} := 1 / \sqrt{\lambda + 1 + \mathbb{E}_{\mathbf{x} \sim \mathbb{P}} \{ \mathbb{E}_{\omega_{\psi_2, \mathbf{z}, \mathbf{z}}} [\|\omega_{\psi_2, \mathbf{z}, \mathbf{z}}\|^2] + \mathbb{E}_{\omega_{\psi_1}} [\|\omega_{\psi_1}\|^2] \} \|\nabla h_{\phi}(\mathbf{x})\|_{\mathcal{F}}^2},$$

and  $\mathbf{z} = h_{\phi}(\mathbf{x})$ .

The derivation can be found in Appendix D. Consequently, by incorporating the conditions in Proposition 5, the objectives for SN-SMMD-GAN-DK are defined as:

$$\min_{\theta} \max_{\phi, \psi} \text{SMMD-DK}_{k, \phi, \psi, \lambda}^2(\mathbb{P}, \mathbb{Q}_{\theta}) \pm \tilde{\Omega}(\theta, \phi, \psi), \quad (12)$$

where  $\tilde{\Omega}(\theta, \phi, \psi) \triangleq \alpha_1 \mathbb{E}_{\omega_{\psi_1}}[\|\omega_{\psi_1}\|^2] + \mathbb{E}_{\omega_{\psi_2, \mathbf{z}_1, \mathbf{z}_2}}[\alpha_2 \|\omega_{\psi_2, \mathbf{z}_1, \mathbf{z}_2}\|^2 + \alpha_3 \|\frac{\partial \omega_{\psi_2, \mathbf{z}_1, \mathbf{z}_2}}{\partial \mathbf{z}_1} - \frac{\partial \omega_{\psi_2, \mathbf{z}_1, \mathbf{z}_2}}{\partial \mathbf{z}_2}\|_{\mathcal{F}}]$ ; and  $\pm$  has the same meaning as that in (11). Note that SMMD has already satisfied continuity in weak-topology, while we found that in SMMD-DK, adding regularizer like 12 would lead to better results.

### 3.3 KernelNet for Implicit Info-VAE

In this section, we describe how to incorporate our KernelNet into the Info-VAE framework. First, to increase the power of Info-VAE, we make the encoder implicit. That is, instead of adopting a particular distribution family such as Gaussian for the encoder, we add random noise at each layer of the encoder (including input data), and transport these simple noise distributions to a complex implicit distribution by the encoder network, as done in GAN. One problem with such a formulation is the need of evaluating the density of the implicit encoder distribution  $q_{\phi}$  for model training, as seen in the original ELBO (1). To deal with this issue, we adopt the Stein gradient estimator (SGE) [15] to approximate the gradient of log-density used in the training.

To introduce our KernelNet into the framework, we notice that mutual information in (1) is essentially a divergence metric between the two distributions  $q_{\phi}(\mathbf{z} | \mathbf{x})$  and  $\mathbf{q}_{\phi}(\mathbf{z})$ . Consequently, we propose to simply replace the mutual information by the MMD parameterized by our KernelNet. The final objective is thus:

$$\begin{aligned} \max_{\phi, \theta, \psi} & -\lambda \text{KL}[q_{\phi}(\mathbf{z}) \| p(\mathbf{z})] - \mathbb{E}_{q_{\phi}(\mathbf{z})} \{ \text{KL}[q_{\phi}(\mathbf{x} | \mathbf{z}) \| p_{\theta}(\mathbf{x} | \mathbf{z})] \} \\ & + \alpha \mathbb{E}_{\mathbf{q}(\mathbf{x})} \{ \text{MMD}_{\kappa_{\psi}}[q_{\phi}(\mathbf{z} | \mathbf{x}), q_{\phi}(\mathbf{z})] \}, \end{aligned}$$

which can be reformulated as:

$$\begin{aligned} \max_{\phi, \theta, \psi} & \mathbb{E}_{q(\mathbf{x})} \mathbb{E}_{q_{\phi}(\mathbf{z} | \mathbf{x})} [\log p_{\theta}(\mathbf{x} | \mathbf{z})] - \mathbb{E}_{q(\mathbf{x})} (\log q_{\mathbf{x}}) \\ & - \mathbb{E}_{q(\mathbf{x})} \{ \text{KL}[q_{\phi}(\mathbf{z} | \mathbf{x}) \| p(\mathbf{z})] \} - (\lambda - 1) \text{KL}[q_{\phi}(\mathbf{z}) \| p(\mathbf{z})] \\ & + \alpha \mathbb{E}_{\mathbf{q}(\mathbf{x})} \{ \text{MMD}_{\kappa_{\psi}}[q_{\phi}(\mathbf{z} | \mathbf{x}), q_{\phi}(\mathbf{z})] \}. \end{aligned} \quad (13)$$

Note that  $\mathbb{E}_{q(\mathbf{x})} (\log q_{\mathbf{x}})$  is independent of the model, and thus can be discarded. When  $\lambda = 1$  and  $\alpha = 0$ , (13) reduces to vanilla VAE.

## 4 Experiments

We conduct experiments to test the performance of our proposed KernelNet applied to MMD-GAN and implicit VAE, and compare them with related methods, including MMD and non-MMD based GANs, parametric and non-parametric implicit VAE models. Our code will be available online.



Figure 2: Generated images on CIFAR-10 ( $32 \times 32$ ).

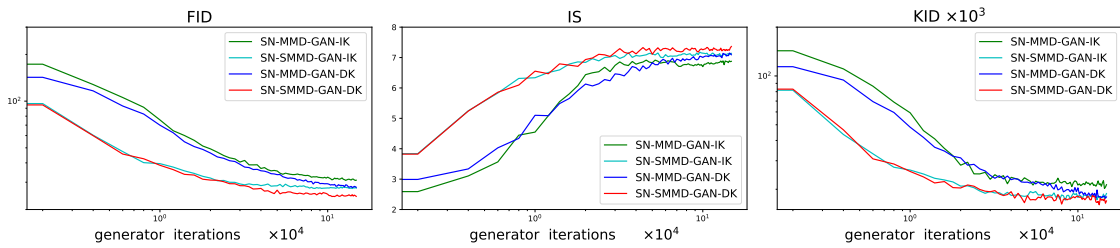


Figure 3: Evaluations of different models.

## 4.1 MMD-GAN

We evaluated our MMD-GAN variants on the CIFAR-10, CelebA [16], and ImageNet [21] datasets. Following Arbel et al. [1], the output dimension of discriminator is set to 1, and inputs of the generator are sampled from a uniform distribution  $\mathcal{U}[-1, 1]^{128}$ . For a fair comparison, all the models are compared under the same architecture in each experiment. Our model architecture follows Arbel et al. [1]. For CIFAR-10, we use an architecture with a 7-layer discriminator and a 4-layer generator. For CelebA, we use a 5-layer discriminator and a 10-layer ResNet generator. For ImageNet, our generator and discriminator are both 10-layer ResNet. We use two 3-layer fully-connected neural networks to parameterize  $\omega_{\psi_1}$  and  $\omega_{\psi_2, \mathbf{z}_1, \mathbf{z}_2}$ . For each neural network, there are 16 neurons in every hidden layer. Spectral normalization [17] is used in SN-MMD-GAN-DK, and spectral parameterization [1] is used in SN-SMMD-GAN-DK.

We use Adam optimizer [10] with a learning rate 0.0001,  $\beta_1 = 0.5$ ,  $\beta_2 = 0.9$  for CIFAR-10 and CelebA, and a learning rate 0.0002,  $\beta_1 = 0.5$ ,  $\beta_2 = 0.999$  for ImageNet. Ratio of learning rate of kernel parameters to learning rate of generator is set to be 0.005. Batch size is 64 for all the models. Models are trained for 150,000 generator update steps for CIFAR-10 and CelebA, 200,000 generator update steps for ImageNet. For every generator step, we update discriminator and kernel parameters 5 steps. At every step, 1024 samples of  $\omega_{\psi_1}$  and  $\omega_{\psi_2}$  are used to compute the values of the kernel function. We set  $\alpha_1 = \alpha_2 = \alpha_3 = 5$  in (11) and  $\alpha_1 = \alpha_2 = \alpha_3 = 0.1$  in (12) for all the experiments.

For evaluation, Fréchet Inception Distance (FID) [9], Inception Score (IS) [23] and Kernel Inception Distance (KID) [3] are computed using 100,000 samples. In every 2,000 generator steps, we compare the model with the one 10,000 steps ago based on the relative KID test [4], and decrease the learning rate by 0.8 if no improvement is found in 3 consecutive times.

The main results are summarized in the Table 1, Table 2 and Table 3, with the generated images shown in Figure 2, Figure 4(a) and Figure 4(b). More results can be found in the Appendix E. Our proposed methods with MMD-based and SMMD-based objectives are denoted as SN-MMD-GAN-DK and SN-SMMD-GAN-DK. For comparison, we also include models using kernels constructed without the data-dependent part, which is the same as the IKL method proposed by Li et al. [14]. These models are denoted as SN-MMD-GAN-IKL and SN-SMMD-GAN-IKL. As we can see, our KernelNet-based models obtain best results than other methods, including the non-MMD-based GAN methods. The results indicate the importance of effectiveness of modeling data dependent kernels with KernelNet. For clearer illustrations, Figure 3 plots the learning curves of score evaluations for different models during the whole training process on CIFAR-10. Example generated images are also illustrated in Figure 4(a) and 4(b).

## 4.2 Implicit VAE

**Multi-modal distribution sampling** We first illustrate the implicit encoder can learn latent variable with multi-mode distributions. This is done by removing the decoder and only training on the encoder, which essentially learns a parametric sampler. We use a 3-layer fully-connected neural network with 20 hidden units as the encoder, whose inputs are Gaussian noises. Figure 4 plots the learned distributions estimated by samples on two target distribution, which can perfectly generates multi-mode samples.



(a) Generated images on CelebA ( $160 \times 160$ ) by SN-SMMD-GAN-DK. (b) Generated images on ImageNet ( $64 \times 64$ ) by SN-SMMD-GAN-DK.

Table 1: Model evaluations on CIFAR-10 dataset.

	IS $\uparrow$	FID $\downarrow$
MMD-GAN	$5.5 \pm 0.1$	$73.9 \pm 0.1$
WGAN-GP	$6.9 \pm 0.2$	$31.1 \pm 0.2$
Sobolev-GAN	$7.0 \pm 0.1$	$30.3 \pm 0.3$
SN-GAN	$7.2 \pm 0.1$	$26.7 \pm 0.2$
SN-SWGAN	$7.2 \pm 0.1$	$28.5 \pm 0.2$
SN-MMD-GAN	$6.9 \pm 0.1$	$31.5 \pm 0.2$
SN-MMD-GAN-IKL	$6.9 \pm 0.1$	$30.4 \pm 0.1$
<b>SN-MMD-GAN-DK</b>	<b><math>7.2 \pm 0.1</math></b>	<b><math>27.8 \pm 0.1</math></b>
SN-SMMD-GAN	$7.3 \pm 0.1$	$25.0 \pm 0.3$
SN-SMMD-GAN-IKL	$7.3 \pm 0.1$	$26.4 \pm 0.1$
<b>SN-SMMD-GAN-DK</b>	<b><math>7.4 \pm 0.1</math></b>	<b><math>24.3 \pm 0.1</math></b>

Table 2: Model evaluations on CelebA dataset.

	IS $\uparrow$	FID $\downarrow$
WGAN-GP	$2.7 \pm 0.1$	$29.2 \pm 0.2$
Sobolev-GAN	$2.9 \pm 0.1$	$16.4 \pm 0.1$
SN-GAN	$2.7 \pm 0.1$	$22.6 \pm 0.1$
SN-SWGAN	$2.8 \pm 0.1$	$14.1 \pm 0.2$
SN-SMMD-GAN	$2.8 \pm 0.1$	$12.4 \pm 0.2$
<b>SN-SMMD-GAN-DK</b>	<b><math>2.9 \pm 0.1</math></b>	<b><math>11.3 \pm 0.1</math></b>

**Implicit VAE** Next, we test our proposed Implicit Info-VAE model on the MNIST dataset [22] to learn an implicit VAE model. We use a fully-connected neural network with 1 hidden layer for both encoder and decoder, whose hidden units are set to 400.  $\omega_{\psi_1}$  and

Table 3: Model evaluations on ImageNet dataset.

	IS $\uparrow$	FID $\downarrow$
BGAN	$10.7 \pm 0.4$	$43.9 \pm 0.3$
SN-GAN	$11.2 \pm 0.1$	$47.5 \pm 0.1$
SMMD-GAN	$10.7 \pm 0.2$	$38.4 \pm 0.3$
SN-SMMD-GAN	$10.9 \pm 0.1$	$36.6 \pm 0.2$
<b>SN-SMMD-GAN-DK</b>	<b><math>11.2 \pm 0.2</math></b>	<b><math>35.7 \pm 0.3</math></b>

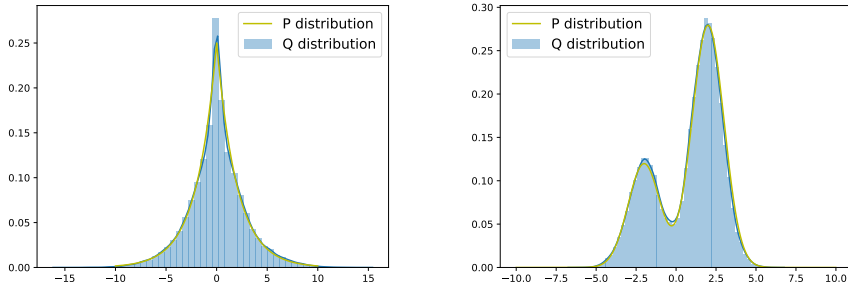


Figure 4: Learning to sample from two target distributions: Laplace(0, 2) (left) and Gaussian mixture  $0.3\mathcal{N}(-2, 1) + 0.7\mathcal{N}(2, 1)$  (right).  $P$ -distribution denotes the ground truth;  $Q$ -distribution denotes the approximated density by samples.

$\omega_{\psi_2, \mathbf{z}_1, \mathbf{z}_2}$  are parameterized by DNNs consisting of 2 fully connected hidden layers with 32 hidden units. Bernoulli noises are injected into the encoder by using dropout with a dropout rate of 0.3. The latent dimension is 32. The models are trained for 300 epochs. Stochastic gradient descent (SGD) with momentum of 0.9 is used with a batch size of 32. We sample 32  $\mathbf{z}$  for every  $\mathbf{x}$ . The learning rate for the encoder and decoder is 0.002, while it is 0.001 for kernel learning. At every step, 512  $\omega_{\psi_1}$  and  $\omega_{\psi_2}$  are sampled. For evaluation, we follow Wu et al. [27] and use Annealed Importance Sampling (AIS) to approximate the negative log-likelihood (NLL). Ten independent AIS chains are used, each of which have 1000 intermediate distributions. The final results are computed using 5000 random sampled test data.

The results are shown in Table 4, where we compare with related models including: *i*) VAE: vanilla VAE; *ii*) Stein-VAE: amortized SVGD [5]; *iii*) SIVI: Semi-Implicit VAE [28]; *iv*) Spectral: implicit VAE with spectral method for gradient estimation [25]; *v*) Info-VAE. We denote our Implicit Info-VAE with Stein gradient estimator with objective (1) as Info-IVAE, and models with objective (13) as Info-IVAE-RBF (i.e., MMD with RBF kernel is used) and Info-IVAE-IK (i.e., MMD with implicit kernel without data-dependent component) and Info-IVAE-DK (i.e., MMD with data-dependent KernelNet), respectively. Note that these model have also reported scores related to NLL in their original paper, which are not directly comparable to ours. For fair comparisons, we use the same encoder-decoder structure and rerun all the models. Our model obtains the best NLL score among all the models. Reconstructed and generated samples are shown in Appendix E.

We also plot the  $t$ -SNE visualization of latent variables learned by Info-IVAE-IK and

Table 4: Negative log-likelihood on the binarized MNIST dataset.

Model	VAE	Stein-VAE	Spectral
NLL ↓	90.32	88.85	89.67
Model	SIVI	Info-VAE	Info-IVAE
NLL ↓	89.03	88.89	89.79
Model	Info-IVAE-RBF	Info-IVAE-IK	Info-IVAE-DK
NLL ↓	88.24	88.21	<b>88.16</b>

Info-IVAE-DK in Figure 5. From the figure we can see that latent variables learned using data-dependent kernel looks more separable than implicit kernel without the data-dependent part. More discussions on Info-VAE experiments can be found in Appendix E. An extra semi-supervised experiment is also presented in Appendix E, where we follow [12] to evaluate the quality of the learned latent variables, and obtain better results.

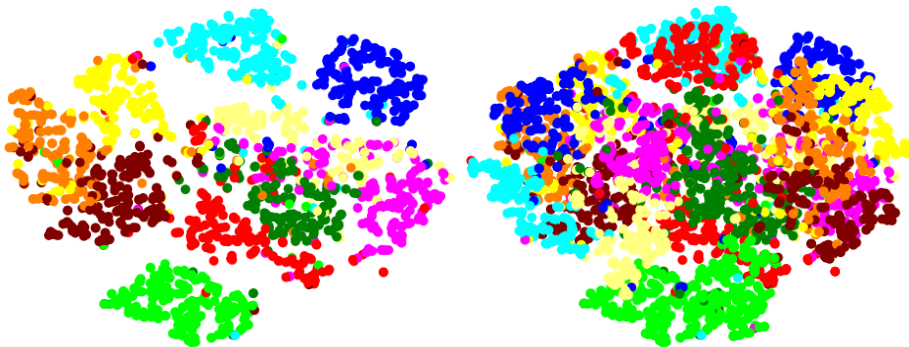


Figure 5: T-SNE visualization of learned latent variables on Mnist, left and right figures correspond to the implicit kernel with/without data-dependent component, respectively.

## 5 Conclusion

We propose KernelNet, a novel way of parameterizing learnable data-dependent kernels using implicit spectral distributions parameterized by DNNs. We analyze how the proposed KernelNet can be applied to deep generative models, including the state-of-the-art variants of MMD-GAN and InfoVAE. Experiments show that the proposed data-dependent KernelNet leads to performance improvement over related models, demonstrating the effectiveness of data-dependent kernels in practice.

## References

- [1] M. Arbel, D. J. Sutherland, M. Binkowski, and A. Gretton. On gradient regularizers for MMD gans. In *Advances in Neural Information Processing Systems 31: Annual Conference on Neural Information Processing Systems 2018, NeurIPS 2018, 3-8 December 2018, Montréal, Canada.*, pages 6701–6711, 2018.
- [2] E. G. Bazavan, F. Li, and C. Sminchisescu. Fourier kernel learning. In *Computer*

- Vision - ECCV 2012 - 12th European Conference on Computer Vision, Florence, Italy, October 7-13, 2012, Proceedings, Part II*, pages 459–473, 2012.
- [3] M. Binkowski, D. J. Sutherland, M. Arbel, and A. Gretton. Demystifying MMD gans. *CoRR*, abs/1801.01401, 2018. URL <http://arxiv.org/abs/1801.01401>.
  - [4] W. Bounliphone, E. Belilovsky, M. B. Blaschko, I. Antonoglou, and A. Gretton. A test of relative similarity for model selection in generative models. In *4th International Conference on Learning Representations, ICLR 2016, San Juan, Puerto Rico, May 2-4, 2016, Conference Track Proceedings*, 2016.
  - [5] Y. Feng, D. Wang, and Q. Liu. Learning to draw samples with amortized stein variational gradient descent. In *UAI*, 2017.
  - [6] M. Gönen and E. Alpaydin. Multiple kernel learning algorithms. *Journal of Machine Learning Research*, 12:2211–2268, 2011. URL <http://dl.acm.org/citation.cfm?id=2021071>.
  - [7] I. Goodfellow, J. Pouget-Abadie, M. Mirza, B. Xu, D. Warde-Farley, S. Ozair, A. Courville, and Y. Bengio. Generative adversarial nets. In *Neural Information Processing Systems (NIPS)*, 2014.
  - [8] I. Gulrajani, F. Ahmed, M. Arjovsky, V. Dumoulin, and A. Courville. Improved training of Wasserstein GANs. In *NIPS*, 2017.
  - [9] M. Heusel, H. Ramsauer, T. Unterthiner, B. Nessler, G. Klambauer, and S. Hochreiter. Gans trained by a two time-scale update rule converge to a nash equilibrium. *CoRR*, abs/1706.08500, 2017. URL <http://arxiv.org/abs/1706.08500>.
  - [10] D. Kingma and J. Ba. Adam: A method for stochastic optimization. In *ICLR*, 2015.
  - [11] D. P. Kingma and M. Welling. Auto-encoding variational Bayes. In *ICLR*, 2014.
  - [12] D. P. Kingma, S. Mohamed, D. J. Rezende, and M. Welling. Semi-supervised learning with deep generative models. In *Advances in Neural Information Processing Systems 27: Annual Conference on Neural Information Processing Systems 2014, December 8-13 2014, Montreal, Quebec, Canada*, pages 3581–3589, 2014. URL <http://papers.nips.cc/paper/5352-semi-supervised-learning-with-deep-generative-models>.
  - [13] C. Li, W. Chang, Y. Cheng, Y. Yang, and B. Póczos. MMD GAN: towards deeper understanding of moment matching network. In *Advances in Neural Information Processing Systems 30: Annual Conference on Neural Information Processing Systems 2017, 4-9 December 2017, Long Beach, CA, USA*, pages 2200–2210, 2017.
  - [14] C. Li, W. Chang, Y. Mroueh, Y. Yang, and B. Póczos. Implicit kernel learning. *CoRR*, abs/1902.10214, 2019. URL <http://arxiv.org/abs/1902.10214>.
  - [15] Y. Li and R. E. Turner. Gradient estimators for implicit models. In *ICLR*, 2018.

- [16] Z. Liu, P. Luo, X. Wang, and X. Tang. Deep learning face attributes in the wild. In *Proceedings of International Conference on Computer Vision (ICCV)*, December 2015.
- [17] T. Miyato, T. Kataoka, M. Koyama, and Y. Yoshida. Spectral normalization for generative adversarial networks. In *6th International Conference on Learning Representations, ICLR 2018, Vancouver, BC, Canada, April 30 - May 3, 2018, Conference Track Proceedings*, 2018.
- [18] A. Rahimi and B. Recht. Random features for large-scale kernel machines. In *NIPS*, 2007.
- [19] D. J. Rezende, S. Mohamed, and D. Wierstra. Stochastic backpropagation and approximate inference in deep generative models. In *ICML*, 2014.
- [20] W. Rudin. *Fourier Analysis on Groups*. Wiley-Interscience, 1994.
- [21] O. Russakovsky, J. Deng, H. Su, J. Krause, S. Satheesh, S. Ma, Z. Huang, A. Karpathy, A. Khosla, M. S. Bernstein, A. C. Berg, and F. Li. Imagenet large scale visual recognition challenge. *International Journal of Computer Vision*, 115(3):211–252, 2015. doi: 10.1007/s11263-015-0816-y. URL <https://doi.org/10.1007/s11263-015-0816-y>.
- [22] R. Salakhutdinov and I. Murray. On the quantitative analysis of deep belief networks. In *Machine Learning, Proceedings of the Twenty-Fifth International Conference (ICML 2008), Helsinki, Finland, June 5-9, 2008*, pages 872–879, 2008.
- [23] T. Salimans, I. Goodfellow, W. Zaremba, V. Cheung, A. Radford, and X. Chen. Improved techniques for training GANs. In *NIPS*, 2016.
- [24] J. Shawe-Taylor and N. Cristianini. *Kernel Methods for Pattern Analysis*. Cambridge University Press, 2004. ISBN 978-0-521-81397-6. URL [http://www.cambridge.org/gb/knowledge/isbn/item1169757/Kernel%20Methods%20for%20Pattern%20Analysis/?site\\_locale=en\\_GB](http://www.cambridge.org/gb/knowledge/isbn/item1169757/Kernel%20Methods%20for%20Pattern%20Analysis/?site_locale=en_GB).
- [25] J. Shi, S. Sun, and J. Zhu. A spectral approach to gradient estimation for implicit distributions. In *Proceedings of the 35th International Conference on Machine Learning*, pages 4651–4660, 2018.
- [26] A. G. Wilson and R. P. Adams. Gaussian process kernels for pattern discovery and extrapolation. In *Proceedings of the 30th International Conference on Machine Learning, ICML 2013, Atlanta, GA, USA, 16-21 June 2013*, pages 1067–1075, 2013.
- [27] Y. Wu, Y. Burda, R. Salakhutdinov, and R. B. Grosse. On the quantitative analysis of decoder-based generative models. *CoRR*, abs/1611.04273, 2016. URL <http://arxiv.org/abs/1611.04273>.
- [28] M. Yin and M. Zhou. Semi-implicit variational inference. In *Proceedings of the 35th International Conference on Machine Learning, ICML 2018, Stockholmsmässan, Stockholm, Sweden, July 10-15, 2018*, pages 5646–5655, 2018.

- [29] S. Zhao, J. Song, and S. Ermon. Infovae: Information maximizing variational autoencoders. *CoRR*, abs/1706.02262, 2017. URL <http://arxiv.org/abs/1706.02262>.

## A Details on proposition 2

By Euler's formula, we have:

$$\kappa(\mathbf{z}_1, \mathbf{z}_2) = \int_{R^d} p(\boldsymbol{\omega}) e^{j\boldsymbol{\omega}^\top(\mathbf{z}_1 - \mathbf{z}_2)} d\boldsymbol{\omega} = \mathbb{E}_{\boldsymbol{\omega}} \{ \cos[\boldsymbol{\omega}^\top(\mathbf{z}_1 - \mathbf{z}_2)] + j \sin[\boldsymbol{\omega}^\top(\mathbf{z}_1 - \mathbf{z}_2)] \}$$

For real-valued kernel, we remove the imaginary part, we have:

$$\kappa(\mathbf{z}_1, \mathbf{z}_2) = \mathbb{E}_{\boldsymbol{\omega}} \{ \cos[\boldsymbol{\omega}^\top(\mathbf{z}_1 - \mathbf{z}_2)] \}$$

Now we show  $\mathbb{E}_{\boldsymbol{\omega}} \{ \cos[\boldsymbol{\omega}^\top(\mathbf{z}_1 - \mathbf{z}_2)] \} = 2\mathbb{E}_{\boldsymbol{\omega}, b} [\cos(\boldsymbol{\omega}^\top \mathbf{z}_1 + b) \cos(\boldsymbol{\omega}^\top \mathbf{z}_2 + b)]$ , where  $b$  follows a uniform distribution  $\mathcal{U}[0, 2\pi]$ :

$$\begin{aligned} & 2\mathbb{E}_{\boldsymbol{\omega}, b} [\cos(\boldsymbol{\omega}^\top \mathbf{z}_1 + b) \cos(\boldsymbol{\omega}^\top \mathbf{z}_2 + b)] \\ &= 2\mathbb{E}_{\boldsymbol{\omega}} \mathbb{E}_b \{ [\cos(\boldsymbol{\omega}^\top \mathbf{z}_1) \cos b - \sin(\boldsymbol{\omega}^\top \mathbf{z}_1) \sin b] [\cos(\boldsymbol{\omega}^\top \mathbf{z}_2) \cos b - \sin(\boldsymbol{\omega}^\top \mathbf{z}_2) \sin b] \} \\ &= 2\mathbb{E}_{\boldsymbol{\omega}} \mathbb{E}_b (\cos \boldsymbol{\omega}^\top \mathbf{z}_1 \cos \boldsymbol{\omega}^\top \mathbf{z}_2 \cos^2 b - \sin \boldsymbol{\omega}^\top \mathbf{z}_1 \cos \boldsymbol{\omega}^\top \mathbf{z}_2 \sin b \cos b \\ &\quad - \cos \boldsymbol{\omega}^\top \mathbf{z}_1 \sin \boldsymbol{\omega}^\top \mathbf{z}_2 \sin b \cos b + \sin \boldsymbol{\omega}^\top \mathbf{z}_1 \sin \boldsymbol{\omega}^\top \mathbf{z}_2 \sin^2 b) \\ &= 2\mathbb{E}_{\boldsymbol{\omega}} \mathbb{E}_b [\cos \boldsymbol{\omega}^\top \mathbf{z}_1 \cos \boldsymbol{\omega}^\top \mathbf{z}_2 \cos^2 b + \sin \boldsymbol{\omega}^\top \mathbf{z}_1 \sin \boldsymbol{\omega}^\top \mathbf{z}_2 \sin^2 b] \\ &\quad - 2\mathbb{E}_{\boldsymbol{\omega}} \mathbb{E}_b [(\sin \boldsymbol{\omega}^\top \mathbf{z}_1 \cos \boldsymbol{\omega}^\top \mathbf{z}_2 - \cos \boldsymbol{\omega}^\top \mathbf{z}_1 \sin \boldsymbol{\omega}^\top \mathbf{z}_2) \sin^2 b] \\ &= 2\mathbb{E}_{\boldsymbol{\omega}} \mathbb{E}_b [\cos \boldsymbol{\omega}^\top \mathbf{z}_1 \cos \boldsymbol{\omega}^\top \mathbf{z}_2 \cos^2 b + \sin \boldsymbol{\omega}^\top \mathbf{z}_1 \sin \boldsymbol{\omega}^\top \mathbf{z}_2 \sin^2 b] \\ &= 2\mathbb{E}_{\boldsymbol{\omega}} \{ \cos \boldsymbol{\omega}^\top \mathbf{z}_1 \cos \boldsymbol{\omega}^\top \mathbf{z}_2 \mathbb{E}_b (\cos 2b + 1) + \sin \boldsymbol{\omega}^\top \mathbf{z}_1 \sin \boldsymbol{\omega}^\top \mathbf{z}_2 \mathbb{E}_b (1 - \cos 2b) \} \\ &= \mathbb{E}_{\boldsymbol{\omega}} [(\cos \boldsymbol{\omega}^\top \mathbf{z}_1 \cos \boldsymbol{\omega}^\top \mathbf{z}_2 + \sin \boldsymbol{\omega}^\top \mathbf{z}_1 \sin \boldsymbol{\omega}^\top \mathbf{z}_2) \mathbb{E}_b (1)] \\ &= \mathbb{E}_{\boldsymbol{\omega}} (\cos \boldsymbol{\omega}^\top \mathbf{z}_1 \cos \boldsymbol{\omega}^\top \mathbf{z}_2 + \sin \boldsymbol{\omega}^\top \mathbf{z}_1 \sin \boldsymbol{\omega}^\top \mathbf{z}_2) \\ &= \mathbb{E}_{\boldsymbol{\omega}} \{ \cos[\boldsymbol{\omega}^\top(\mathbf{z}_1 - \mathbf{z}_2)] \} \end{aligned}$$

The proposition has been proved.

## B Existence of data-dependent kernel

Consider a symmetric positive definite kernel defined on manifold  $M \subset R^d$  (e.g. heat kernel), whose value depends on geodesic distance between 2 points rather than Euclidean distance.

For two pairs  $(\mathbf{z}_1, \mathbf{z}_2)$  and  $(\mathbf{z}_3, \mathbf{z}_4)$ , if  $\mathbf{z}_1 - \mathbf{z}_2 = \mathbf{z}_3 - \mathbf{z}_4$ , we may have  $\kappa(\mathbf{z}_1, \mathbf{z}_2) \neq \kappa(\mathbf{z}_3, \mathbf{z}_4)$ . With abuse of notation, we may write the kernel as  $\kappa(\mathbf{z}_1, \mathbf{z}_2) = f(\mathbf{z}_c)$ , where we use  $\mathbf{z}_c = [\mathbf{z}_1, \mathbf{z}_2]$  to denote the concatenation of  $\mathbf{z}_1$  and  $\mathbf{z}_2$ . Now the corresponding positive definite function  $f(\mathbf{z}_c)$  is a mapping from  $R^{2d}$  to  $R$ , rather than from  $R^d$  to  $R$ .

According to Lemma 1, we can write the kernel as

$$\kappa(\mathbf{z}_1, \mathbf{z}_2) = f(\mathbf{z}_c) = \mathbb{E}_{\boldsymbol{\tau}} [e^{j\boldsymbol{\tau}^\top \mathbf{z}_c}]$$

where  $\boldsymbol{\tau} \in R^{2d}$ . If there exists  $\boldsymbol{\omega} \in R^d$  such that

$$\mathbb{E}_{\boldsymbol{\tau}} [e^{j\boldsymbol{\tau}^\top \mathbf{z}_c}] = \mathbb{E}_{\boldsymbol{\omega}} [e^{j\boldsymbol{\omega}^\top(\mathbf{z}_1 - \mathbf{z}_2)}]$$

$p(\boldsymbol{\omega})$  has to be data-dependent, otherwise we'll have  $\kappa(\mathbf{z}_1, \mathbf{z}_2) = \kappa(\mathbf{z}_3, \mathbf{z}_4)$  in the previous example, which contradicts with the fact.

Now we show why there always exists  $\boldsymbol{\omega}$  such that  $\boldsymbol{\tau}^\top \mathbf{z}_c = \boldsymbol{\omega}^\top (\mathbf{z}_1 - \mathbf{z}_2)$  for any  $\boldsymbol{\tau}, \mathbf{z}_1, \mathbf{z}_2$ . One can regard  $\boldsymbol{\tau}^\top \mathbf{z}_c = \boldsymbol{\omega}^\top (\mathbf{z}_1 - \mathbf{z}_2)$  as system of linear equations  $A\boldsymbol{\omega} = b$ , where  $\boldsymbol{\omega}$  is unknown.

Denote  $b = \boldsymbol{\tau}^\top \mathbf{z}_c$ , we can regard  $A = (\mathbf{z}_1 - \mathbf{z}_2)^\top$  as coefficient matrix and  $B = [A, b]$  as augmented matrix. Because  $0 \leq \text{rank}(A) \leq \text{rank}(B) \leq 1 \leq d$ . If  $\text{rank}(A) = 1$ , then there must be 1 or infinite solutions, hence  $\boldsymbol{\omega}$  exists; If  $\text{rank}(A) = 0$ , we can conclude that  $\mathbf{z}_1 = \mathbf{z}_2$ . Simply setting  $\boldsymbol{\tau} = [\boldsymbol{\omega}, -\boldsymbol{\omega}]$ , i.e. the concatenation of two vectors, then  $\boldsymbol{\tau}^\top \mathbf{z}_c = \boldsymbol{\omega}^\top (\mathbf{z}_1 - \mathbf{z}_2)$  always holds for any  $\boldsymbol{\omega}$ . Thus we can always write  $\boldsymbol{\tau}^\top \mathbf{z}_c = \boldsymbol{\omega}^\top (\mathbf{z}_1 - \mathbf{z}_2)$ .

Two additional notes: (1). Note that  $f(\mathbf{z}_c)$  may not be defined everywhere on  $\mathbb{R}^{2d}$ , but this problem is easy to handle, as when  $\mathbf{z}_1$  or  $\mathbf{z}_2 \notin M$ , we can simply set  $f(\mathbf{z}_c) = 0$ , the resulting function is still positive definite; (2). We want to rewrite  $\mathbb{E}_{\boldsymbol{\tau}}[e^{j\boldsymbol{\tau}^\top \mathbf{z}_c}] = \mathbb{E}_{\boldsymbol{\omega}}[e^{j\boldsymbol{\omega}^\top (\mathbf{z}_1 - \mathbf{z}_2)}]$ , because this is the easiest way to maintain the symmetry of kernel, i.e.  $\kappa(\mathbf{z}_1, \mathbf{z}_2) = \kappa(\mathbf{z}_2, \mathbf{z}_1)$ .

## C Proof of proposition 5

We start from the following Lemma:

**Lemma 7 ([1])** *Assume the critic functions, which have form:*

$$f_{\boldsymbol{\nu}}(\mathbf{a}) = (\mathbb{E}_{\mathbf{x} \sim \mathbb{P}} k_{\boldsymbol{\nu}}(\mathbf{x}, \mathbf{a}) - \mathbb{E}_{\mathbf{y} \sim \mathbb{Q}} k_{\boldsymbol{\nu}}(\mathbf{y}, \mathbf{a})) / \text{MMD}_{k_{\boldsymbol{\nu}}}(\mathbb{P}, \mathbb{Q})$$

*are uniformly bounded and have a common Lipschitz constant:*

$$\sup_{\mathbf{a} \in \mathbb{R}^D, \boldsymbol{\nu} \in V} |f_{\boldsymbol{\nu}}(\mathbf{a})| < \infty \quad \sup_{\boldsymbol{\nu} \in V} \|f_{\boldsymbol{\nu}}(\mathbf{a})\|_{Lip} < \infty.$$

*Then  $\text{MMD}_{k_{\boldsymbol{\nu}}}(\mathbb{P}, \mathbb{Q})$  is continuous in the weak topology. In particular, this holds when  $k_{\boldsymbol{\nu}} = \kappa \circ h_{\phi}$  and*

$$\sup_{\mathbf{z} \in \mathbb{R}^d} \kappa(\mathbf{z}, \mathbf{z}) < \infty, \quad \|\kappa(\mathbf{z}_1, \cdot) - \kappa(\mathbf{z}_2, \cdot)\|_{\mathcal{H}_{\kappa}} \leq L_{\kappa} \|\mathbf{z}_1 - \mathbf{z}_2\|_{\mathbb{R}^d}, \quad \sup_{\phi \in \Phi} \|h_{\phi}\|_{Lip} < \infty$$

From (2) we know that  $\sup_{\mathbf{z}_1 \in \mathbb{R}^d} \kappa_{\psi}(\mathbf{z}_1, \mathbf{z}_1) < \infty$  is naturally satisfied. We prove the second condition in Lemma 7 here:

$$\begin{aligned} & \|\kappa_{\psi}(\mathbf{z}_1, \cdot) - \kappa_{\psi}(\mathbf{z}_2, \cdot)\|_{\mathcal{H}} \\ & \leq \sqrt{\langle \kappa_{\psi}(\mathbf{z}_1, \cdot) - \kappa_{\psi}(\mathbf{z}_2, \cdot), \kappa_{\psi}(\mathbf{z}_1, \cdot) - \kappa_{\psi}(\mathbf{z}_2, \cdot) \rangle_{\mathcal{H}}} \\ & = \sqrt{\kappa_{\psi}(\mathbf{z}_1, \mathbf{z}_1) + \kappa_{\psi}(\mathbf{z}_2, \mathbf{z}_2) - 2\kappa_{\psi}(\mathbf{z}_1, \mathbf{z}_2)} \\ & = \sqrt{\kappa_{\psi_1}(\mathbf{z}_1, \mathbf{z}_1) + \kappa_{\psi_1}(\mathbf{z}_2, \mathbf{z}_2) - 2\kappa_{\psi_1}(\mathbf{z}_1, \mathbf{z}_2) + \kappa_{\psi_2}(\mathbf{z}_1, \mathbf{z}_1) + \kappa_{\psi_2}(\mathbf{z}_2, \mathbf{z}_2) - 2\kappa_{\psi_2}(\mathbf{z}_1, \mathbf{z}_2)} \\ & \leq \sqrt{2 - 2\kappa_{\psi_1}(\mathbf{z}_1, \mathbf{z}_2)} + \sqrt{2 - 2\kappa_{\psi_2}(\mathbf{z}_1, \mathbf{z}_2)} \end{aligned} \tag{14}$$

Let start with the second term above, denote  $f_2(\mathbf{t}) = 2 - \kappa_2(\mathbf{t})$ , where  $\mathbf{t} = \mathbf{z}_1 - \mathbf{z}_2$ .

$$\begin{aligned}
& \|\nabla_{\mathbf{t}} f_2(\mathbf{t})\| \\
&= \|\nabla_{\mathbf{t}} [2 - 2\kappa_{\psi_2}(\mathbf{t})]\| \\
&= \|\nabla_{\mathbf{t}} \{2 - 2\mathbb{E}_{\omega_{\psi_2, \mathbf{t}}} [\cos(\omega_{\psi_2, \mathbf{t}}^\top \mathbf{t})]\}\| \\
&= 2\|\mathbb{E}_{\omega_{\psi_2, \mathbf{t}}} [\sin(\omega_{\psi_2, \mathbf{t}}^\top \mathbf{t}) (\omega_{\psi_2, \mathbf{t}}^\top + \mathbf{t} \nabla_{\mathbf{t}} \omega_{\psi_2, \mathbf{t}})]\| \\
&\leq 2\|\mathbb{E}_{\omega_{\psi_2, \mathbf{t}}} [\sin(\omega_{\psi_2, \mathbf{t}}^\top \mathbf{t}) \omega_{\psi_2, \mathbf{t}}]\| + 2\|\mathbb{E}_{\omega_{\psi_2, \mathbf{t}}} [\sin(\omega_{\psi_2, \mathbf{t}}^\top \mathbf{t}) \mathbf{t} \nabla_{\mathbf{t}} \omega_{\psi_2, \mathbf{t}}]\| \\
&\leq 2\mathbb{E}_{\omega_{\psi_2, \mathbf{t}}} (\|\mathbf{t}\| \|\omega_{\psi_2, \mathbf{t}}\|^2) + 2\mathbb{E}_{\omega_{\psi_2, \mathbf{t}}} (\|\mathbf{t}\| \|\nabla_{\mathbf{t}} \omega_{\psi_2, \mathbf{t}}\|_{\mathcal{F}}) \\
&= 2\mathbb{E}_{\omega_{\psi_2, \mathbf{t}}} [\|\mathbf{t}\| (\|\omega_{\psi_2, \mathbf{t}}\|^2 + \|\nabla_{\mathbf{t}} \omega_{\psi_2, \mathbf{t}}\|_{\mathcal{F}})]
\end{aligned}$$

If  $2\mathbb{E}_{\omega_{\psi_2, \mathbf{t}}} [\|\omega_{\psi_2, \mathbf{t}}\|^2] \leq c_1$  and  $2\mathbb{E}_{\omega_{\psi_2, \mathbf{t}}} [\|\nabla_{\mathbf{t}} \omega_{\psi_2, \mathbf{t}}\|_{\mathcal{F}}] \leq c_2$ , for constants  $c_1, c_2$ , then we have  $\|\nabla_{\mathbf{t}} f_2(\mathbf{t})\| \leq c\|\mathbf{t}\|$ , where  $c = c_1 + c_2$ .

$$\begin{aligned}
\|f_2(\mathbf{t})\| &= \left\| \int \nabla_{\mathbf{t}} f_2(\mathbf{t}) d\mathbf{t} \right\| = \int \|\nabla_{\mathbf{t}} f_2(\mathbf{t})\| d\mathbf{t} \\
&\leq c \int \|\mathbf{t}\| d\mathbf{t} = c \int \sqrt{\sum_{i=1}^d t_i^2} d\mathbf{t} \\
&\leq c \sum_{i=1}^d \int |t_i| dt_i \\
&\leq c \sum_{i=1}^d \frac{t_i^2}{2} = \frac{c}{2} \|\mathbf{t}\|^2
\end{aligned}$$

Thus we can conclude, if

$$\mathbb{E}_{\omega_{\psi_2, \mathbf{t}}} [\|\omega_{\psi_2, \mathbf{t}}\|^2] < \infty, \quad \mathbb{E}_{\omega_{\psi_2, \mathbf{t}}} [\|\nabla_{\mathbf{t}} \omega_{\psi_2, \mathbf{t}}\|_{\mathcal{F}}] < \infty$$

then  $\sqrt{f_2(\mathbf{t})} \leq \sqrt{\frac{c}{2}} \|\mathbf{t}\|$  holds. Similar result can be easily get for the first term in (14). Then we can conclude if:

$$\mathbb{E}_{\omega_{\psi_1}} [\|\omega_{\psi_1}\|^2] < \infty, \quad \mathbb{E}_{\omega_{\psi_2, \mathbf{t}}} [\|\omega_{\psi_2, \mathbf{t}}\|^2] < \infty, \quad \mathbb{E}_{\omega_{\psi_2, \mathbf{t}}} [\|\nabla_{\mathbf{t}} \omega_{\psi_2, \mathbf{t}}\|_{\mathcal{F}}] < \infty \quad (15)$$

then

$$\|\kappa_{\psi}(\mathbf{z}_1, \cdot) - \kappa_{\psi}(\mathbf{z}_2, \cdot)\|_{\mathcal{H}} \leq L_{\kappa} \|\mathbf{t}\| = L_{\kappa} \|\mathbf{z}_1 - \mathbf{z}_2\|$$

For some constant  $L_{\kappa}$ . Because  $\mathbf{t} = \mathbf{z}_1 - \mathbf{z}_2$ , we have:

$$\nabla_{\mathbf{t}} \omega_{\psi_2, \mathbf{t}} = \frac{\partial \omega_{\psi_2, \mathbf{z}_1, \mathbf{z}_2}}{\partial \mathbf{z}_1} \frac{\partial \mathbf{z}_1}{\partial \mathbf{t}} + \frac{\partial \omega_{\psi_2, \mathbf{z}_1, \mathbf{z}_2}}{\partial \mathbf{z}_2} \frac{\partial \mathbf{z}_2}{\partial \mathbf{t}} = \frac{\partial \omega_{\psi_2, \mathbf{z}_1, \mathbf{z}_2}}{\partial \mathbf{z}_1} - \frac{\partial \omega_{\psi_2, \mathbf{z}_1, \mathbf{z}_2}}{\partial \mathbf{z}_2} \quad (16)$$

Substitute (16) into (15), proposition 5 is proved.

## D Details on proposition 6

In our data-dependent kernel setting,  $k = \kappa_{\psi} \circ h_{\phi}$ , hence we write  $k(\mathbf{y}, \mathbf{z}) = \kappa_{\psi}(h_{\phi}(\mathbf{y}), h_{\phi}(\mathbf{z}))$ , where  $h_{\phi}$  is the discriminator, and  $\kappa_{\psi}$  is the proposed data-dependent kernel. For our

data-dependent kernel, we know that

$$\int \kappa_{\psi, \phi}(\mathbf{x}, \mathbf{x}) d\mathbb{P}(\mathbf{x}) = 1$$

from (2).

$$\begin{aligned} & \sum_{i=1}^d \int \frac{\partial^2 \kappa_{\psi}(\mathbf{y}_1, \mathbf{y}_2)}{\partial \mathbf{y}_{1i} \partial \mathbf{y}_{2i}} \Big|_{(\mathbf{y}_1, \mathbf{y}_2) = (\mathbf{x}, \mathbf{x})} d\mathbb{P}(\mathbf{x}) \\ &= \sum_{i=1}^d \int \frac{\partial^2 \kappa_{\psi_1}(\mathbf{y}_1, \mathbf{y}_2)}{\partial \mathbf{y}_{1i} \partial \mathbf{y}_{2i}} \Big|_{(\mathbf{y}_1, \mathbf{y}_2) = (\mathbf{x}, \mathbf{x})} d\mathbb{P}(\mathbf{x}) + \sum_{i=1}^d \int \frac{\partial^2 \kappa_{\psi_2}(\mathbf{y}_1, \mathbf{y}_2)}{\partial \mathbf{y}_{1i} \partial \mathbf{y}_{2i}} \Big|_{(\mathbf{y}_1, \mathbf{y}_2) = (\mathbf{x}, \mathbf{x})} d\mathbb{P}(\mathbf{x}) \end{aligned}$$

where  $\mathbf{z}_1 = h_{\phi}(\mathbf{y}_1)$  and  $\mathbf{z}_2 = h_{\phi}(\mathbf{y}_2)$ . For clearness, we will write  $\boldsymbol{\omega}_{\psi_2}$  instead of  $\boldsymbol{\omega}_{\psi_2, \mathbf{z}_1, \mathbf{z}_2}$ , but please keep in mind that  $\boldsymbol{\omega}_{\psi_2}$  is dependent on the input data. Because of the reparameterization trick, we can write  $\mathbb{E}_{\epsilon \sim \mathcal{N}(\mathbf{0}, \mathbf{I})}(\cdot)$  instead of  $\mathbb{E}_{\boldsymbol{\omega}_{\psi, \mathbf{z}_1, \mathbf{z}_2}}(\cdot)$ ,

$$\begin{aligned} & \sum_{i=1}^d \int \frac{\partial^2 \kappa_{\psi_2}(\mathbf{y}_1, \mathbf{y}_2)}{\partial \mathbf{y}_{1i} \partial \mathbf{y}_{2i}} \Big|_{(\mathbf{y}_1, \mathbf{y}_2) = (\mathbf{x}, \mathbf{x})} d\mathbb{P}(\mathbf{x}) \\ &= \sum_{i=1}^d \int \frac{\partial^2 \mathbb{E}_{\epsilon \sim \mathcal{N}(\mathbf{0}, \mathbf{I})} \{ \cos \{ \boldsymbol{\omega}_{\psi_2}^{\top} [h_{\phi}(\mathbf{y}_1) - h_{\phi}(\mathbf{y}_2)] \} \}}{\partial \mathbf{y}_{1i} \partial \mathbf{y}_{2i}} \Big|_{(\mathbf{y}_1, \mathbf{y}_2) = (\mathbf{x}, \mathbf{x})} d\mathbb{P}(\mathbf{x}) \\ &= \sum_{i=1}^d \int \int \frac{\partial}{\partial \mathbf{y}_{2i}} \sin \{ \boldsymbol{\omega}_{\psi_2}^{\top} [h_{\phi}(\mathbf{y}_1) - h_{\phi}(\mathbf{y}_2)] \} \\ & \quad \left\{ \frac{\partial \boldsymbol{\omega}_{\psi_2}}{\partial \mathbf{y}_{1i}}^{\top} [h_{\phi}(\mathbf{y}_1) - h_{\phi}(\mathbf{y}_2)] + \boldsymbol{\omega}_{\psi_2}^{\top} \frac{\partial h_{\phi}(\mathbf{y}_1)}{\partial \mathbf{y}_{1i}} \right\} d\boldsymbol{\mu}(\boldsymbol{\epsilon}) \Big|_{(\mathbf{y}_1, \mathbf{y}_2) = (\mathbf{x}, \mathbf{x})} d\mathbb{P}(\mathbf{x}) \\ &= \sum_{i=1}^d \int \int -\cos \{ \boldsymbol{\omega}_{\psi_2}^{\top} [h_{\phi}(\mathbf{y}_1) - h_{\phi}(\mathbf{y}_2)] \} \left\{ \frac{\partial \boldsymbol{\omega}_{\psi_2}}{\partial \mathbf{y}_{2i}}^{\top} [h_{\phi}(\mathbf{y}_1) - h_{\phi}(\mathbf{y}_2)] + \boldsymbol{\omega}_{\psi_2}^{\top} \left[ -\frac{\partial h_{\phi}(\mathbf{y}_2)}{\partial \mathbf{y}_{2i}} \right] \right\} \\ & \quad \times \left\{ \frac{\partial \boldsymbol{\omega}_{\psi_2}}{\partial \mathbf{y}_{1i}}^{\top} [h_{\phi}(\mathbf{y}_1) - h_{\phi}(\mathbf{y}_2)] + \boldsymbol{\omega}_{\psi_2}^{\top} \frac{\partial h_{\phi}(\mathbf{y}_1)}{\partial \mathbf{y}_{1i}} \right\} \\ & \quad + \sin \{ \boldsymbol{\omega}_{\psi_2}^{\top} [h_{\phi}(\mathbf{y}_1) - h_{\phi}(\mathbf{y}_2)] \} \frac{\partial}{\partial \mathbf{y}_{2i}} \left\{ \frac{\boldsymbol{\omega}_{\psi_2}}{\partial \mathbf{y}_{1i}}^{\top} [h_{\phi}(\mathbf{y}_1) - h_{\phi}(\mathbf{y}_2)] + \boldsymbol{\omega}_{\psi_2}^{\top} \frac{\partial h_{\phi}(\mathbf{y}_1)}{\partial \mathbf{y}_{1i}} \right\} d\boldsymbol{\mu}(\boldsymbol{\epsilon}) \Big|_{(\mathbf{y}_1, \mathbf{y}_2) = (\mathbf{x}, \mathbf{x})} d\mathbb{P}(\mathbf{x}) \\ &= \sum_{i=1}^d \int \int [\boldsymbol{\omega}_{\psi_2, \mathbf{z}, \mathbf{z}}^{\top} \frac{\partial h_{\phi}(\mathbf{x})}{\partial \mathbf{x}_i}]^2 d\boldsymbol{\mu}(\boldsymbol{\epsilon}) d\mathbb{P}(\mathbf{x}) \end{aligned}$$

where  $\mathbf{z} = h_{\phi}(\mathbf{x})$ . In our experiment, the output dimension of discriminator  $h_{\phi}$  is set to be 1. Then the result becomes:

$$\sum_{i=1}^d \int \frac{\partial^2 \kappa_{\psi_2, \mathbf{z}_1, \mathbf{z}_2}(\mathbf{y}_1, \mathbf{y}_2)}{\partial \mathbf{y}_{1i} \partial \mathbf{y}_{2i}} \Big|_{(\mathbf{y}_1, \mathbf{y}_2) = (\mathbf{x}, \mathbf{x})} d\mathbb{P}(\mathbf{x}) = \mathbb{E}_{\mathbf{x} \sim \mathbb{P}} \{ \mathbb{E}_{\boldsymbol{\omega}_{\psi_2, \mathbf{z}, \mathbf{z}}} [ \| \boldsymbol{\omega}_{\psi_2, \mathbf{z}, \mathbf{z}} \|^2 ] \| \nabla h_{\phi}(\mathbf{x}) \|_{\mathcal{F}} \}$$

Similarly, we have:

$$\sum_{i=1}^d \int \frac{\partial^2 \kappa_{\psi_1}(\mathbf{y}_1, \mathbf{y}_2)}{\partial \mathbf{y}_{1i} \partial \mathbf{y}_{2i}} \Big|_{(\mathbf{y}_1, \mathbf{y}_2) = (\mathbf{x}, \mathbf{x})} d\mathbb{P}(\mathbf{x}) = \mathbb{E}_{\mathbf{x} \sim \mathbb{P}} \{ \mathbb{E}_{\boldsymbol{\omega}_{\psi_1}} [ \| \boldsymbol{\omega}_{\psi_1} \|^2 ] \| \nabla h_{\phi}(\mathbf{x}) \|_{\mathcal{F}} \}$$

Hence:

$$\begin{aligned} & \sum_{i=1}^d \int \frac{\partial^2 \kappa_{\omega}(\mathbf{y}_1, \mathbf{y}_2)}{\partial \mathbf{y}_{1i} \partial \mathbf{y}_{2i}} \Big|_{(\mathbf{y}_1, \mathbf{y}_2) = (\mathbf{x}, \mathbf{x})} d\mathbb{P}(\mathbf{x}) \\ &= \mathbb{E}_{\mathbf{x} \sim \mathbb{P}} \{ \{ \mathbb{E}_{\omega_{\psi_2, \mathbf{z}, \mathbf{z}}} [\|\omega_{\psi_2, \mathbf{z}, \mathbf{z}}\|^2] + \mathbb{E}_{\omega_{\psi_1}} [\|\omega_{\psi_1}\|^2] \} \|\nabla h_{\phi}(\mathbf{x})\|_{\mathcal{F}} \} \end{aligned} \quad (17)$$

## E Experiments results and discussion

### E.1 MMD-GAN

In practice, we choose  $\lambda$  and scale the original SMMD-DK objective so that

$$\widehat{\text{SMMD-DK}}_{k_{\psi}, \phi, \lambda}^2(\mathbb{P}, \mathbb{Q}) = \frac{\sigma_{k_{\psi}, \phi, \lambda} \text{MMD}_{k_{\psi}}^2(\mathbb{P}, \mathbb{Q})}{1 + 5 \mathbb{E}_{\mathbf{x} \sim \mathbb{P}} \{ \{ \mathbb{E}_{\omega_{\psi_2, \mathbf{z}, \mathbf{z}}} [\|\omega_{\psi_2, \mathbf{z}, \mathbf{z}}\|^2] + \mathbb{E}_{\omega_{\psi_1}} [\|\omega_{\psi_1}\|^2] \} \|\nabla h_{\phi}(\mathbf{x})\|_{\mathcal{F}} \}}$$

is used in in (12).

Here are some more detailed results of MMD-GAN experiments, including results from more models and KID evaluation.

Table 5: Model evaluations on CIFAR-10 dataset.

	IS $\uparrow$	FID $\downarrow$	KID $\times 10^3 \downarrow$
MMD-GAN	$5.5 \pm 0.1$	$73.9 \pm 0.1$	$39.4 \pm 1.5$
WGAN-GP	$6.9 \pm 0.2$	$31.1 \pm 0.2$	$22.2 \pm 1.1$
Sobolev-GAN	$7.0 \pm 0.1$	$30.3 \pm 0.3$	$22.3 \pm 1.2$
SN-GAN	$7.2 \pm 0.1$	$26.7 \pm 0.2$	$16.1 \pm 0.9$
SN-SWGAN	$7.2 \pm 0.1$	$28.5 \pm 0.2$	$17.6 \pm 1.1$
SN-MMD-GAN	$6.9 \pm 0.1$	$31.5 \pm 0.2$	$21.7 \pm 1.0$
SN-MMD-GAN-GP	$4.6 \pm 0.1$	$96.8 \pm 0.4$	$59.5 \pm 1.4$
SN-MMD-GAN-L2	$7.1 \pm 0.1$	$31.9 \pm 0.2$	$21.7 \pm 0.9$
SN-MMD-GAN-GP-L2	$6.9 \pm 0.2$	$32.3 \pm 0.3$	$20.9 \pm 1.1$
SN-MMD-GAN-IKL	$6.9 \pm 0.1$	$30.4 \pm 0.1$	$20.6 \pm 1.6$
<b>SN-MMD-GAN-DK (Ours)</b>	<b><math>7.2 \pm 0.1</math></b>	<b><math>27.8 \pm 0.1</math></b>	<b><math>17.3 \pm 1.4</math></b>
SN-SMMD-GAN	$7.3 \pm 0.1$	$25.0 \pm 0.3$	$16.6 \pm 2.0$
SN-SMMD-GAN-IKL	$7.3 \pm 0.1$	$26.4 \pm 0.1$	$16.8 \pm 1.2$
<b>SN-SMMD-GAN-DK (Ours)</b>	<b><math>7.4 \pm 0.1</math></b>	<b><math>24.3 \pm 0.1</math></b>	<b><math>16.0 \pm 0.8</math></b>

Table 6: Model evaluations on CelebA dataset.

	IS $\uparrow$	FID $\downarrow$	KID $\times 10^3 \downarrow$
WGAN-GP	$2.7 \pm 0.1$	$29.2 \pm 0.2$	$22.0 \pm 1.0$
Sobolev-GAN	$2.9 \pm 0.1$	$16.4 \pm 0.1$	$10.6 \pm 0.5$
SN-GAN	$2.7 \pm 0.1$	$22.6 \pm 0.1$	$14.6 \pm 1.1$
SN-SWGAN	$2.8 \pm 0.1$	$14.1 \pm 0.2$	$7.7 \pm 0.5$
SN-SMMD-GAN	$2.8 \pm 0.1$	$12.4 \pm 0.2$	<b><math>6.1 \pm 0.4</math></b>
<b>SN-SMMD-GAN-DK (Ours)</b>	<b><math>2.9 \pm 0.1</math></b>	<b><math>11.3 \pm 0.1</math></b>	$6.7 \pm 0.6$

Table 7: Model evaluations on ImageNet dataset.

	IS $\uparrow$	FID $\downarrow$	KID $\times 10^3 \downarrow$
BGAN	$10.7 \pm 0.4$	$43.9 \pm 0.3$	$47.0 \pm 1.1$
SN-GAN	$11.2 \pm 0.1$	$47.5 \pm 0.1$	$44.4 \pm 2.2$
SMMD-GAN	$10.7 \pm 0.2$	$38.4 \pm 0.3$	$39.3 \pm 2.5$
SN-SMMD-GAN	$10.9 \pm 0.1$	$36.6 \pm 0.2$	<b><math>34.6 \pm 1.6</math></b>
<b>SN-SMMD-GAN-DK (Ours)</b>	<b><math>11.2 \pm 0.2</math></b>	<b><math>35.7 \pm 0.3</math></b>	$38.6 \pm 1.5$

## E.2 Info-VAE

Mutual information between two distributions is easy to be handled only in certain situations, e.g. both of them are Gaussian. If one considers the implicit VAE setting, one has to design some non-trivial methods to deal with the intractability of the mutual information. One possible choice is to use an implicit gradient estimator to estimate the implicit distribution’s gradient, then use it for optimization. However, this is very inaccurate and unstable in our preliminary studies. By replacing the MI with MMD (the logic is quite straightforward because both MMD and MI can be reconsidered as distance measures of two distributions), it is much easier to be dealt with, because MMD can be computed based on samples.

We show some reconstructed images and generated images from the Info-VAE experiment in Figure 6.

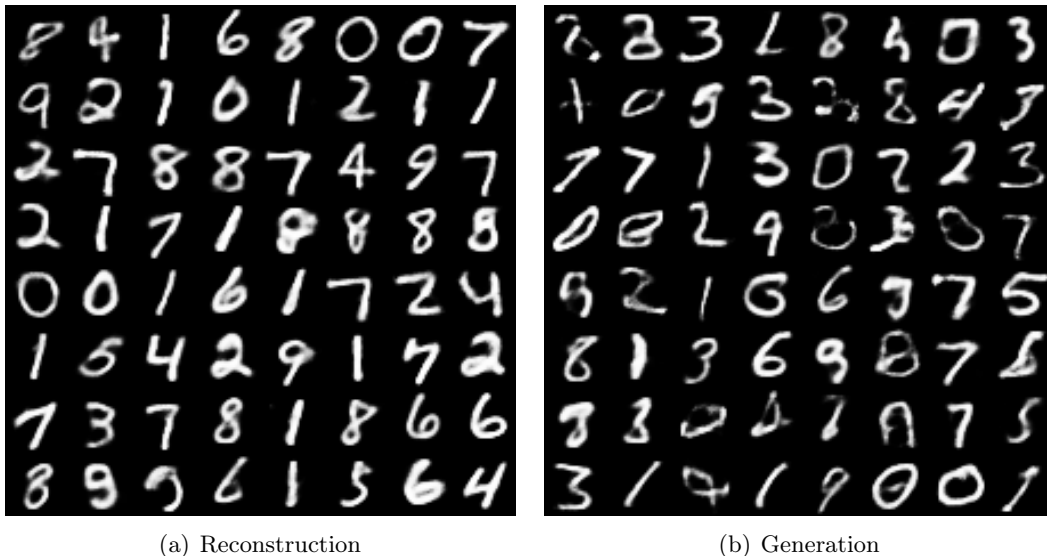


Figure 6: Reconstructed and generated images on MNIST.

We also evaluate the latent variables learned by Info-IVAE with different kernels following [12]. After we finish training Info-IVAE models, we generate latent features using the encoders. Then we train a SVM on these latent features. More informative latent variables should lead to better classification performance, the results are shown in Figure 7.

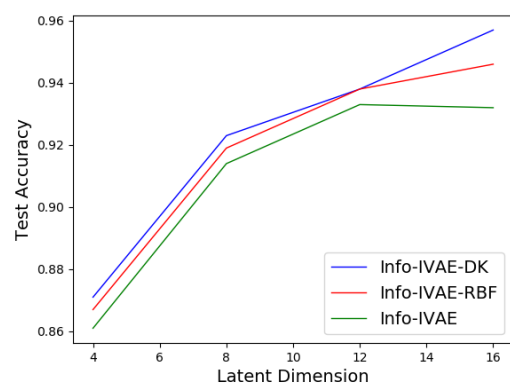


Figure 7: Semi-supervised experiment on Mnist dataset